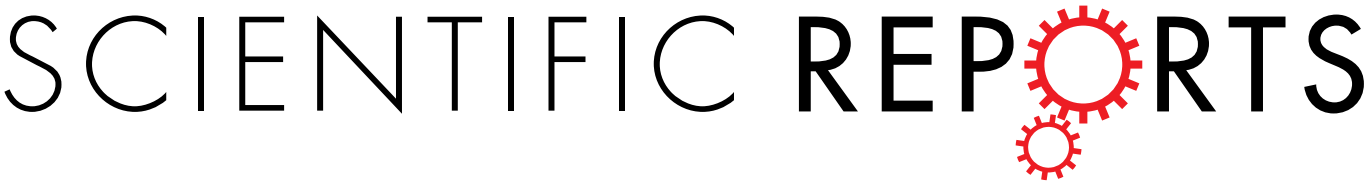

OPEN

# New insight into magneto-structural phase transitions in layered $TbMn_2Ge_2$-based compounds

Received: 02 September 2016
Accepted: 06 March 2017
Published: 04 April 2017

Chunsheng Fang[1], Guoxing Li[1,2], Jianli Wang[1,3], W. D. Hutchison[4], Q. Y. Ren[4], Zhenyan Deng[5], Guohong Ma[5], Shixue Dou[1], S. J. Campbell[4] & Zhenxiang Cheng[1]

**The $Tb_{1-x}Y_xMn_2Ge_2$ series ($x = 0, 0.1, 0.2$) compounds are found to exhibit two magnetic phase transitions with decreasing temperature: from the paramagnetic state to the antiferromagnetic interlayer state at $T_N^{inter}$ and from an antiferromagnetic interlayer structure to a collinear ferrimagnetic interlayer structure at $T_C^{inter}$. Compared with the slight change of $T_N^{inter}$ (409 K, 410 K and 417 K for $x = 0$, 0.1 and 0.2 respectively), the replacement of Y for Tb leads to a significant decrease in $T_C^{inter}$ from 97.5 K for $x = 0$ to 74.6 K for $x = 0.2$. The variation in $T_C^{inter}$ can be ascribed to the combination of two effects: (1) chemical pressure and (2) magnetic dilution effect by Y substitution for Tb. Besides, a strong anisotropic magnet-volume effect has been detected around $T_C^{inter}$ in all compounds with $\Delta a/a = 0.125\%$, 0.124% and 0.130% for $x = 0$, 0.1 and 0.2, respectively while no obvious effect is detected along the c-axis. The maximum magnetic entropy change were found to be $-\Delta S_{max} = 9.1\,J\,kg^{-1}\,K^{-1}$, $11.9\,J\,kg^{-1}\,K^{-1}$ and $6.3\,J\,kg^{-1}\,K^{-1}$ with a field change from 0T to 5T for $x = 0$, 0.1, 0.2 respectively.**

Since the discovery in 1997 of a giant magnetocaloric effect (GMCE) originating from a discontinuous first order magnetic transition in $Gd_5Si_2Ge_2$[1], room-temperature magnetic refrigeration based on the magnetocaloric effect (MCE) has attracted significant attention due to its energy efficiency and environment friendly in comparison with conventional gas compression-expansion refrigeration[2]. A number of materials which exhibit giant magnetic entropy changes at magnetic transitions have been investigated, including $MnFeP_{0.45}As_{0.55}$[3], $MnAs_{1-x}Sb_x$[4], Ni-Mn-Sn-based alloys[5], Ni-Mn-Ga[6,7], and $La(Fe,Si)_{13}$[8]. The key features of these systems are the temperature- and magnetic field-induced first-order magneto-structural or magneto-elastic phase transitions. Given these promising developments, magnetic materials which exhibit a large magnetocaloric effect have been studied extensively, both experimentally and theoretically, over the past two decades with the overall aim of increasing the efficiency of magnetic refrigeration techniques[9,10]. While a key focus is exploration of materials that exhibit a pronounced magnetocaloric effect at room temperature, materials that operate in the low temperature region are also useful in meeting the cooling requirements for fields such as gas liquefaction or attaining millikelvin for experimental research facilities. However, so far only a few materials such as $GdLiF_4$, $GdF_3$ and $Gd_3Ga_5O_{12}$ are used commercially[11]. As reflected by the increase in exploration of materials which exhibit a large MCE below room temperature[10–13], the search for materials which exhibit large magnetocaloric effects over temperature ranges relevant for hydrogen and natural gas liquefaction are also important for exploring potential applications.

Some $RT_2X_2$ compounds (R = rare earth, T = transition metal, and X = Si or Ge) have been found to exhibit large MCE values with small hysteresis losses near their low magnetic transition temperatures[11,13–16]. For example, the magnetic entropy values of $RNi_2Si_2$ (R = Dy, Ho, Er) compounds are $21.3\,J\,kg^{-1}\,K^{-1}$, $21.7\,J\,kg^{-1}\,K^{-1}$ and $22.9\,J\,kg^{-1}\,K^{-1}$ around 6.5 K, 4.5 K and 3.5 K respectively during a change of magnetic induction intensity from

[1]Institute for Superconducting and Electronic Materials, Innovation Campus, University of Wollongong, NSW 2500, Australia. [2]State Key Laboratory on Integrated Optoelectronics, College of Electronic Science and Engineering, Jilin University, Changchun 130012, People's Republic of China. [3]College of Physics, Jilin University, Changchun 130012, People's Republic of China. [4]School of Physical, Environmental and Mathematical Sciences, UNSW Canberra at the Australian Defence Force Academy, ACT 2600, Australia. [5]Department of Physics, Shanghai University, 99 Shangda Road, Shanghai, 200444, China. Correspondence and requests for materials should be addressed to J.W. (email: jianli@uow.edu.au) or Z.C. (email: cheng@uow.edu.au)

0–5 T[16], while the magnetic entropy of $ErCr_2Si_2$ attained 29.7 J kg$^{-1}$ K$^{-1}$ near the magnetic ordering temperature 4.5 K[17]. The crystal structure of the $RT_2X_2$ series is body centred tetragonal $ThCr_2Si_2$-type (with space group I4/mmm)[15,18,19], with the sequence -R-X-T-X-R- atomic layers stacked along the c-axis. The rare earth elements typically exhibit large magnetic moment (for example $\mu_{Tb} = 8.8\,\mu_B$ in $TbMn_2Si_2$ at 5 K)[20] and correspondingly make a large contribution to the magnetocaloric effect[14,15,17]. Given the sensitivity of the magnetic state in $RMn_2X_2$ to the intra-planar Mn-Mn spacing[15,19,21–24], compounds in this series are found to display a rich variety of interesting phenomena, including superconductivity, magnetism, mixed valence, heavy fermions, and Kondo behaviour[25–27]. This diversity enables control of the interplay between the R-Mn and Mn-Mn exchange interactions in $RMn_2X_2$ through external factors such as pressure[28], temperature and magnetic field[29] meaning that such compounds have the potential for competitive performance[15,19,24]. The notations used in this paper to describe the magnetic structure type and critical transition temperatures are defined by Venturini *et al.*[22] Using standard magnetic methods[19,30], $TbMn_2Ge_2$ was reported to be antiferromagnetic below Néel temperature $T_N = 410$ K with the AFil antiferromagnetic interlayer structure (*i.e.* a collinear antiferromagnetic structure between adjacent Mn planes in a $+--+$ sequence along the *c*-axis[22].) Below $T_C = 100$ K, $TbMn_2Ge_2$ exhibits a collinear ferrimagnetic structure in which the Tb moments order ferromagnetically and couple antiferromagnetically with the Mn moment[23]. Furthermore, in a later study for the $Tb_{1-x}Y_xMn_2Ge_2$ series (x = 0–0.4), it was reported that the replacement of Y for Tb leads to significant modifications of both the Curie temperature (from 76 K for $TbMn_2Ge_2$ to almost 0 K for $Tb_{0.4}Y_{0.6}Mn_2Ge_2$) and magnetovolume effect (the volume effect is $\Delta V/V = 3.2 \times 10^{-3}$ and $2.7 \times 10^{-3}$ for x = 0 and 0.1 respectively)[30]. The magnetic phase transitions around $T_C$ in the Tb-rich $Tb_{1-x}Y_xMn_2Ge_2$ compounds were shown to be first order[30], offering scope for large magnetocaloric effects around the region of their Curie temperatures.

Here we present a systematic study of the magnetic transition from antiferromagnetism to ferromagnetism in a series of $Tb_{1-x}Y_xMn_2Ge_2$ samples (x = 0, 0.1, 0.2) using a combination of methods including variable temperature x-ray diffraction (XRD), specific heat, differential scanning calorimetry (DSC) and magnetization measurements. The overall aim is to understand fully the influence of Y substitution for Tb on magnetocaloric effects and search for novel magnetocaloric materials that may be suitable for operation over the hydrogen and natural gas liquefaction temperature ranges.

## Method

The polycrystalline $Tb_{1-x}Y_xMn_2Ge_2$ samples with x = 0, 0.1, 0.2 were prepared by arc melting constituent elements of 99.9% purity under argon atmosphere. For improved crystallization and chemical homogeneity, the samples were annealed in vacuum-sealed quartz tube at 850 °C for 7 days after arc melting. The dc magnetic measurements were performed using a Quantum Design 9 T physical properties measurement system (PPMS). The magnetic behaviour was investigated over the range from 5 K to 340 K in a magnetic field 0.01 T. Differential scanning calorimetry measurements were performed on differential scanning calorimetry equipment (DSC 204 ***F1** Phoenix®*) from 340 K to 500 K. Magnetization-field loops were obtained at temperatures close to the Curie temperature of samples with magnetic fields over the range 0–5 T. The heat capacity measurements were performed on a Quantum Design 14 T physical properties measurement system scanning from 2 K to 250 K. The samples were characterized and the structures determined by variable temperatures XRD measurements over the temperature range (12–300 K) using a PANAlytical diffractometer with Cu-K$\alpha$ radiation.

## Results and Discussion

**Structural behaviour.** The room temperature x-ray diffraction study shows that all samples are single phase and that patterns can be indexed with a space group of I4/mmm as expected. The Rietveld refinements have been carried out using the FullProf package[31] with the main results shown in Fig. 1(a,b and c) for x = 0, 0.1 and 0.2 respectively. It can be seen from Fig. 1. that the variations of lattice parameters of *a* and *c* with temperature display strong anisotropy: the lattice parameter *c* (red solid circle) increases monotonically with increasing temperature while a pronounced discontinuity is observed in the *a* lattice parameter (black solid square) around the Curie temperature $T_c$ for each sample (the transition temperatures were determined as the point where the value of dM/dT is minimum). Similar behaviours for $TbMn_2Ge_2$ were also determined by Morellon *et al.*[23] for which an anomaly in the thermal expansion along the *a*-axis was found near $T_c$. The discontinuity in the *a* lattice parameter around $T_c$ leads to the associated decrease in the unit cell volume for all samples as also evident in Fig. 1. These behaviours are very similar to the behaviour reported for $Pr_{0.5}Y_{0.5}Mn_2Ge_2$[15] (i.e. $PrMn_2Ge_2$ diluted by Y), but different from $NdMn_2Ge_{0.4}Si_{1.6}$[32], $NdMn_{1.9}Ti_{0.1}Si_2$[33] and $NdMn_{1.7}Cr_{0.3}Si_2$[34,35] (where Mn diluted with transition metal Ti or Ge diluted by Si) for which the lattice parameter *a* decreases with increasing temperature around $T_C$ while the lattice parameter *c* expands. In order to derive the magneto-volume effect below $T_C$, we have calculated the contribution from lattice vibration using the Debye model:

$$\beta = k\gamma C_v/V \tag{1}$$

where $\beta$ is the volume thermal expansion coefficient of the parameter state, k is the compressibility, $\gamma$ is the Gruneisen constant and $C_v$ is the specific heat at constant volume caused by lattice vibrations. $C_v$ was derived from the Debye theory of the specific heat using the value of the Debye temperature $^{\theta}{}_D$ (as derived from our specific heat measurements for each of the samples as described below for the three compositions):

$$C_v = 9Nk_B\left(\frac{T}{\theta_D}\right)^3 \int_0^{\theta_D/T} \frac{x^4 e^x}{(e^x - 1)^2} dx \tag{2}$$

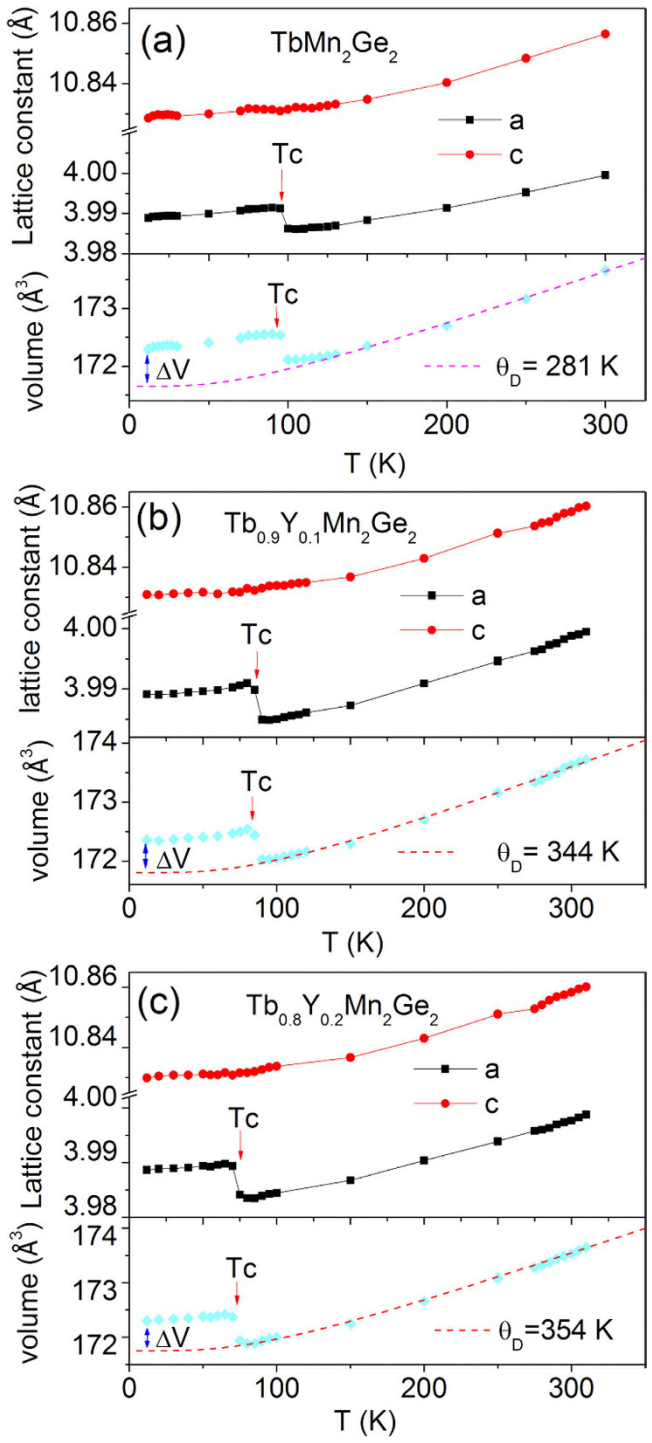


**Figure 1.** Temperature dependence of the lattice constants a, c and unit cell volume: (**a**) $TbMn_2Ge_2$, (**b**) $Tb_{0.9}Y_{0.1}Mn_2Ge_2$ and (**c**) $Tb_{0.8}Y_{0.2}Mn_2Ge_2$. The dashed lines show the phonon contribution to the lattice expansion as evaluated from the Gruneisen relation.

where $k_B$ is the Boltzmann constant and N is the number of the atoms. The thermal expansion for the hypothetical paramagnetic state is derived on integrating Eq. (2) with respect to temperature. The parameter $k\gamma/V$ was adjusted to obtain the best least-squares fitting to the successive data points of the observed thermal expansion curve well above the magnetic ordering temperature (based on the fact that the magnetic contribution in the antiferromagnetic region to total thermal expansion can be ignored for these types of compounds)[32].

The temperature dependence of the unit cell volumes based on Debye theory for the $TbMn_2Ge_2$, $Tb_{0.9}Y_{0.1}Mn_2Ge_2$ and $Tb_{0.8}Y_{0.2}Mn_2Ge_2$ samples are shown by the dashed lines in Fig. 1(a,b and c) with pronounced magneto-volume effects evident below their magnetic transition temperatures $T_C = 94$ K, $T_C = 83$ K and $T_C = 70$ K respectively. The discontinuous nature of the changes in *a* lattice parameter and unit cell volume *V* at the Curie

temperatures as shown in Fig. 1, are consistent with the first order nature of these transitions as discussed fully below. The changes in the lattice parameter *a* are $\Delta a/a = 0.125\%$, $\Delta a/a = 0.124\%$ and $\Delta a/a = 0.130\%$ for $x = 0, 0.1$ and 0.2 respectively with spontaneous volume magnetostriction $\omega_s$ ($=\Delta V_m/V$) at 5 K determined as: $TbMn_2Ge_2$ - $\omega_s = 4.1 \times 10^{-3}$; $Tb_{0.9}Y_{0.1}Mn_2Ge_2$ - $\omega_s = 3.2 \times 10^{-3}$ and $Tb_{0.8}Y_{0.2}Mn_2Ge_2$ - $\omega_s = 5.8 \times 10^{-3}$.

**Magnetic phase transition.** The magnetisation of the three samples have been measured in a field of B = 0.01 T over the temperature range 5–340 K. As in Fig. 2(a,b and c) the $TbMn_2Ge_2$, $Tb_{0.9}Y_{0.1}Mn_2Ge_2$ and $Tb_{0.8}Y_{0.2}Mn_2Ge_2$ samples were respectively measured on warming from 5 K in three states: after cooling in zero field (ZFC heating) and after cooling and heating in a field of B = 0.01 T (FC cooling and FC heating). As is evident from the magnetization versus temperature curves of Fig. 2(a,b and c), there is an abrupt change in magnetisation at the Curie temperature $T_C^{inter}$ that marks the magnetic phase transition from a collinear antiferromagnetism (AFil)[22] at higher temperature to a collinear ferrimagnetic structure along the *c* axis at lower temperature according to the neutron diffraction study on $TbMn_2Ge_2$[23]. Of the three samples, $TbMn_2Ge_2$ has the highest $T_C^{inter}(warm) = 97.5$ K and $T_C^{inter}(cool) = 93.0$ K transitions respectively as determined from the FC heating and cooling M-T curves, while the values for $Tb_{0.9}Y_{0.1}Mn_2Ge_2$ are derived to be $T_C^{inter}(warm) = 87.5$ K and $T_C^{inter}(cool) = 81.8$ K with the values for $Tb_{0.8}Y_{0.2}Mn_2Ge_2$ being $T_C^{inter}(warm) = 74.6$ K and $T_C^{inter}$ cool) = 66.0 K (normally the transition temperature during the FC process is chosen as the Curie temperature $T_c$). As expected, the higher the level of doping of non-magnetic Y atoms in $Tb_{1-x}Y_xMn_2Ge_2$, the lower the magnetic phase transition temperature[30].

Differential scanning calorimetry measurements have been carried out on the $Tb_{1-x}Y_xMn_2Ge_2$ samples over the temperature range 300–500 K (Fig. 2(d)) in order to investigate the paramagnetic to antiferromagnetic transition[10,23] at $T_N^{inter}$. As revealed by the DSC results in Fig. 2(d), the $T_N^{inter}$ transition temperatures are found to increase slightly with increasing Y concentration - $T_N^{inter} = 409$ K, $T_N^{inter} = 410$ K and $T_N^{inter} = 417$ K for $x = 0.0$, 0.1 and 0.2 respectively. Compared with the reduction in ferromagnetic transition temperature on replacement of Tb atoms by Y atoms, the paramagnetic to antiferromagnetic transition temperatures are found to exhibit a slight increase (Fig. 2). The increase in $T_N^{inter}$ values is due to enhancement of the Mn-Mn exchange interaction as a result of the slight reduction of Mn-Mn distance. This behaviour is similar to the $PrMn_2Ge_{2-x}Si_x$ system[36] in which the paramagnetic to antiferromagnetic transition temperatures are found to increase slightly while the antiferromagnetic to ferromagnetic transition temperatures decrease on replacing Ge with Si.

The temperature dependences of magnetization for $TbMn_2Ge_2$, $Tb_{0.9}Y_{0.1}Mn_2Ge_2$ and $Tb_{0.8}Y_{0.2}Mn_2Ge_2$ under various external magnetic fields are presented in Fig 3(a,b and c) respectively. As expected the ferromagnetic transition temperature $T_C^{inter}$ is shifted to higher temperature with increase in applied magnetic field. For example, the transition temperatures are $T_C^{inter} = 101.8$ K, $T_C^{inter} = 92$ K and $T_C^{inter} = 76$ K for $TbMn_2Ge_2$, $Tb_{0.9}Y_{0.1}Mn_2Ge_2$ and $Tb_{0.8}Y_{0.2}Mn_2Ge_2$ respectively in an external magnetic field of B = 1 T, while the transition temperatures are shifted to $T_C^{inter} = 107$ K, $T_C^{inter} = 98.2$ K and $T_C^{inter} = 81$ K respectively in a field of B = 5 T. The field dependence of the magnetic transition temperatures are summarized in Fig. 3(d). The values of $dT_c/dB$ (obtained on linear fitting of the experimental data in Fig. 3(d) along with a summary of experimental data determined for $Tb_{1-x}Y_xMn_2Ge_2$ ($x = 0, 0.1, 0.2$) in this investigation, are provided in Table 1.

**Y doping in $Tb_{1-x}Y_xMn_2Ge_2$ - Chemical pressure effect.** As noted above, the effect of replacing the magnetic rare earth Tb with the nonmagnetic ion Y in $Tb_{1-x}Y_xMn_2Ge_2$ is to weaken the exchange interaction between magnetic ions due to the dilution effect. The magnetic behaviour of Y-doped $Tb_{1-x}Y_xMn_2Ge_2$ will also be modified as a result of chemical pressure due to differences in the atomic radii of the Tb(1.80 Å) and Y(1.78 Å) ions and resultant changes in lattice parameters. In order to separate these two contributions - dilution effect and pressure effect - and their influence on the variation in magnetic transition temperature, the decrease of $T_C$ by chemical pressure was calculated as follows. The chemical pressure $\Delta p$ was calculated[20,22,33] according to the Murnaghan equation below:

$$\Delta p(V) = \frac{B_0}{B_0'}\left(\left(\frac{V_0}{V}\right)^{B_0'} - 1\right) \tag{3}$$

where $V_0$, $B_0$ and $B_0'$ are the volume, the bulk modulus and its first derivative of $TbMn_2Ge_2$ and V is the volume of the unit cell at room temperature of the Y doped samples. Here, due to the similarity of crystal structure for the $RMn_2Ge_2$ system, we assume that the values of $B_0$ and $B_0'$ for $PrMn_2Ge_2$ ($B_0 = 38.0$ Gpa, $B_0' = 19.5$ as derived from our synchrotron data under external pressure[37]) can be applied to $TbMn_2Ge_2$ at room temperature. Given that the doped materials $Tb_{1-x}Y_xMn_2Ge_2$ ($x = 0.1, 0.2$) retain the $ThCr_2Si_2$-type tetragonal structure, the chemical pressure $\Delta p$ caused by doping can be assumed to have the same effect as mechanical pressure. According to previous findings that describe the pressure effect on the magnetic properties of $TbMn_2Ge_2$ ($dT_c/dP = -2.9$ K/kbar)[38], the values of $\Delta T_C$ can be deduced by the relationship:

$$\Delta T_c^{chemical} = dT_c/dp * \Delta p \tag{4}$$

where $\Delta p$ is the calculated chemical pressure. The calculated values of $\Delta T_C$ for $Tb_{0.9}Y_{0.1}Mn_2Ge_2$ and $Tb_{0.8}Y_{0.2}Mn_2Ge_2$ are $\Delta T_C = 1.94$ K and $\Delta T_C = 8.7$ K respectively. As noted above (see also Fig. 1, Figs 2 and 3.) the effect of replacing Tb atoms with Y atoms in $Tb_{1-x}Y_xMn_2Ge_2$ also contributes to the decrease in the Curie temperature. It can therefore be concluded that chemical pressure accounts for ~17.3% and ~32.2% of the decrease in transition temperatures for $x = 0.1$ and 0.2 respectively. In addition, the value of $dT_c/dp$ can be derived using the Clausius-Clapeyron thermodynamic relation as follows:[15]

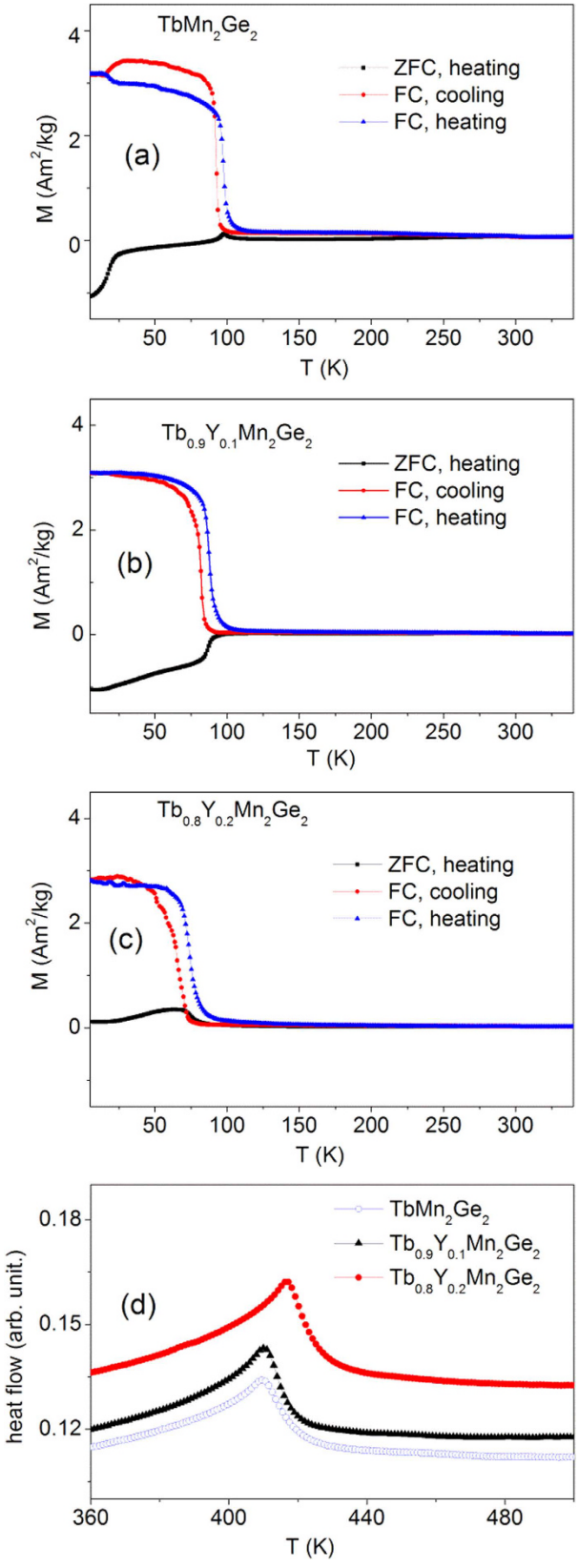


**Figure 2.** Temperature dependence of magnetization on ZFC heating, FC cooling and FC heating processes under a field of B = 0.01 T: (**a**) $TbMn_2Ge_2$, (**b**) $Tb_{0.9}Y_{0.1}Mn_2Ge_2$ and (**c**) $Tb_{0.8}Y_{0.2}Mn_2Ge_2$. (**d**) the differential scanning calorimetry curves for the three samples over the range ~300–500 K.

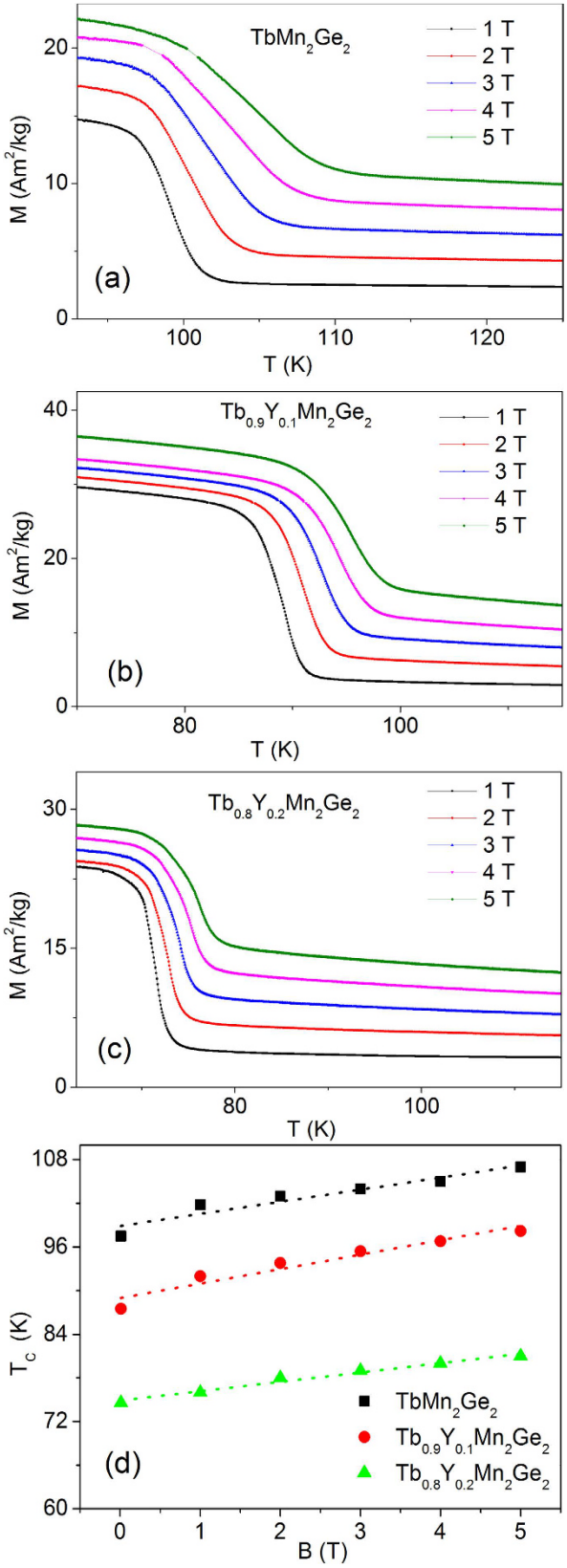


**Figure 3. The magnetisation versus temperature curves during cooling under various magnetic field (B = 1–5 T).** (**a**) $TbMn_2Ge_2$, (**b**) $Tb_{0.9}Y_{0.1}Mn_2Ge_2$, (**c**) $Tb_{0.8}Y_{0.2}Mn_2Ge_2$. (**d**) The variation of ferromagnetic transition temperature $T_c$ with magnetic field for the three samples. The dashed lines represent linear fits to the $T_c$-B curves leading to $dT_c/dB$ values for each sample.

| x | 0 | 0.1 | 0.2 |
|---|---|---|---|
| $\Delta$p (Gpa) | 0 | 0.012 | 0.053 |
| V (Å$^3$)(300 K) | 173.66(5) | 173.63 | 173.53 |
| V (Å$^3$) | 0.40 | 0.52 | 0.54 |
| $\Delta\mu$ (Am$^2$/kg) (B = 1 T) | 14.0(5) | 28.2 | 22.7 |
| experimental $T_c$ (K) (FC) | 93.0(5) | 81.8 | 66.0 |
| $\Delta T_c^{chemical}$ (K) | 0 | 1.94 | 8.70 |
| $\Delta T_c^{total}$ (K) | 0 | 11.2 | 27.0 |
| $\Delta T_c^{chemical}/\Delta T_c^{total}$ | 0 | 17.3% | 32.2% |
| $dT_c$/dB (cooling) (K/T) (FC) | 1.06 ± 0.04 | 1.54 ± 0.05 | 1.29 ± 0.09 |
| $dT_c$/dp (K/kbar) (FC) | −3.03 | −2.84 | −3.07 |

**Table 1. Experimental data for the three $Tb_{1-x}Y_xMn_2Ge_2$ samples (x = 0, 0.1 and 0.2).** Y composition x, chemical pressure $\Delta$p, unit cell volume at 300 K, the change in unit cell volume $\Delta V_m$ and the change in moment $\Delta\mu$ on magnetic field 1 T during the structural transition, value of $T_c$ during the FC process, the value of $dT_c$/dB, the total difference value of Curie temperature $\Delta T_c^{total}$ between $Tb_{1-x}Y_xMn_2Ge_2$ (x = 0.1 and 0.2) and $TbMn_2Ge_2$, the derived values of $\Delta T_c^{chemical}$ (caused by chemical pressure) and $dT_c$/dp of $Tb_{1-x}Y_xMn_2Ge_2$ (x = 0, 0.1 and 0.2). The errors are shown for the $TbMn_2Ge_2$ data as an example.

$$\frac{dT_c}{dp} = -\Delta V_m/\Delta M * \left(\frac{dT_c}{dB}\right). \quad (5)$$

The values of the change in the unit cell volume $\Delta V_m$ he change in moment $\Delta\mu$ during magnetic phase transition around $T_C$ and $dT_c$/dB for each sample were taken from the present experimental results listed in Table.1. The derived results are dT/dp = −3.03 K/kbar, −2.84 K/kbar and −3.07 K/kbar for $TbMn_2Ge_2$, $Tb_{0.9}Y_{0.1}Mn_2Ge_2$ and $Tb_{0.8}Y_{0.2}Mn_2Ge_2$, respectively. These calculated values are in general accord with the value of $dT_c/dp = -2.9$ K/kbar for $TbMn_2Ge_2$[38], deviating by ~4.5%, ~2.1% and ~5.9% for the x = 0.0. 0.1, 0.2 samples respectively.

**Magnetocaloric effect.** Graphs of the magnetization as a function of applied field are shown for $TbMn_2Ge_2$, $Tb_{0.9}Y_{0.1}Mn_2Ge_2$, and $Tb_{0.8}Y_{0.2}Mn_2Ge_2$ at temperatures around $T_C^{inter}$ in Fig. 4(a,b and c) respectively. It can be seen that with increasing temperature beyond $T_C^{inter}$, a field-induced metamagnetic phase transition from the antiferromagnetic state to the ferromagnetic state at certain temperatures has been detected. The region of the metamagnetic phase transition for $TbMn_2Ge_2$ is indicated by arrows in Fig. 4(a) as a typical example. This behaviour indicates that the region of ferromagnetic ordering in $Tb_{1-x}Y_xMn_2Ge_2$ can be shifted to higher temperatures by a stronger applied magnetic field.

The nature of the magnetic transitions (first order or second order) was analysed using Arrott plots with the magnetisation expressed in the usual way as graphs of $M^2$ versus B/M (Fig. 5). As can be seen in Fig. 5(a,b and c), negative slopes are detected in the $M^2$ versus B/M graphs for the $TbMn_2Ge_2$ and $Tb_{0.9}Y_{0.1}Mn_2Ge_2$ samples thus indicating that the antiferromagnetic to ferromagnetic processes are first order[39]. However, Some papers[40,41] reported that for compounds near the critical point (from first order to second order magnetic phase transition) such as $DyCo_2$, this criterion of Arrott plots do not always work properly. It is also noted that the negative slopes for $Tb_{0.8}Y_{0.2}Mn_2Ge_2$ around the antiferromagnetic to ferromagnetic transition was reduced compared with those for the $TbMn_2Ge_2$ and $Tb_{0.9}Y_{0.1}Mn_2Ge_2$ samples. However, the first order transition characters of all the three samples can be confirmed from our variable temperatures crystal structure analyses above, where strong magneto-elastic coupling around $T_C^{inter}$ has been detected (Fig. 1).

The magnetic entropy changes $\Delta S_M$ for all samples have been determined from the isothermal magnetization curves of Fig. 4(a,b and c), by using the standard Maxwell relationship:

$$\Delta S_M(T, B) = \int_0^{B^{max}} \left(\frac{\partial M(B, T)}{\partial T}\right)_B dB. \quad (6)$$

The calculated temperature dependent magnetic entropy changes for the $Tb_{1-x}Y_xMn_2Ge_2$ samples with x = 0, 0.1 and 0.2 for both increasing field and decreasing field processes between field changes of $\Delta B = 0$–1 T and $\Delta B = 0$–5 T are shown in Fig. 6(a,b and c) respectively with the maximum values $\Delta S_{max}$ shown as a function of applied field in the insets of Fig. 6. With a field change of $\Delta B = 0$–5 T, the value of $-\Delta S_{max}$ are 9.1 J/kgK, 11.9 J/kgK and 6.3 J/kgK for $TbMn_2Ge_2$, $Tb_{0.9}Y_{0.1}Mn_2Ge_2$ and $Tb_{0.8}Y_{0.2}Mn_2Ge_2$ respectively, demonstrating that the entropy change for $Tb_{0.9}Y_{0.1}Mn_2Ge_2$ is the largest of the three samples. As it is clear from Fig. 4, while $TbMn_2Ge_2$ has the highest fraction of magnetic rare earth element and largest saturation magnetization (42.5 Am$^2$/kg at 84 K), its large hysteresis loss (7.40 J/kg) leads to reduction in the magnetic entropy change. By comparison, with the lowest concentration of magnetic rare earth Tb, the $Tb_{0.8}Y_{0.2}Mn_2Ge_2$ sample displays the lowest saturation magnetization (only 32.5 Am$^2$/kg even at 55 K) and the smallest hysteresis loss 5.21 J/kg), while as shown in Fig. 4(b), $Tb_{0.9}Y_{0.1}Mn_2Ge_2$ with medium concentration of Tb has a relatively large saturation magnetization of 38.0 Am$^2$/Kg at 84 K and small hysteresis loss (5.36 J/kg). The refrigerant capacity (RCP), defined as the product of $-\Delta S_{max}$ and the full width at half maximum of the $-\Delta S_{max}$ curve, for the three samples are: 93.3 J/kg, 102.9 J/kg,

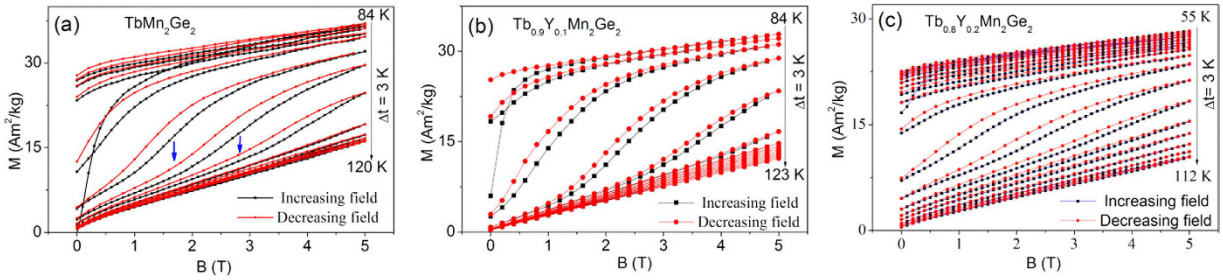


**Figure 4. Curves of isothermal magnetization versus magnetic field at temperatures around $T_c$.** (**a**) $TbMn_2Ge_2$, (**b**) $Tb_{0.9}Y_{0.1}Mn_2Ge_2$ and (**c**) $Tb_{0.8}Y_{0.2}Mn_2Ge_2$.

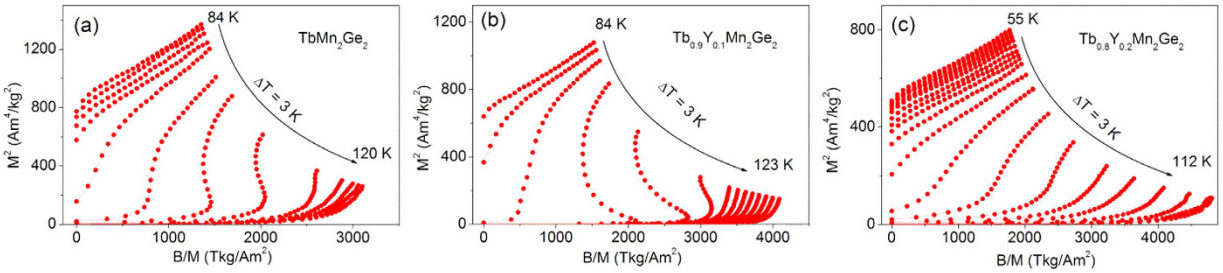


**Figure 5. Arrott plots: isotherms graphs of $M^2$ versus B/M for decreasing magnetic fields at temperatures around $T_c$.** (**a**) $TbMn_2Ge_2$, (**b**) $Tb_{0.9}Y_{0.1}Mn_2Ge_2$ and (**c**) $Tb_{0.8}Y_{0.2}Mn_2Ge_2$.

62.4 J/kg for $TbMn_2Ge_2$, $Tb_{0.9}Y_{0.1}Mn_2Ge_2$ and $Tb_{0.8}Y_{0.2}Mn_2Ge_2$ respectively, with a field change of $\Delta B = 0$–5 T. The MCE value of $Tb_{0.9}Y_{0.1}Mn_2Ge_2$ is comparable to those of other materials for a field change of $\Delta B = 0$–5 T including: GdCoAl, $-\Delta S_{max}(T) = 10.4$ J/kgK at 100 K[34], TbCoAl, $-\Delta S_{max}(T) = 10.5$ J/kgK at 70 K[34] and $GdMn_2Ge_2$, $-\Delta S_{max}(T) = 1.2$ J/kgK at 95 K[28], all of which, in common with $Tb_{0.9}Y_{0.1}Mn_2Ge_2$, importantly exhibit negligible field and thermal hysteresis losses.

Moreover, it is well accepted that first-order phase transitions are accompanied by a latent heat and the barocaloric effect can be expected. In fact giant barocaloric effect has been found in several systems recently including $Mn_3GaN$ ($\Delta S_{bar} = 22.3$ J/K kg)[42] and Ni–Mn–In magnetic superelastic alloys ($\Delta S_{bar} = 27.7$ J/K kg)[43]. Based on the fact that all these three $Tb_{1-x}Y_xMn_2Ge_2$ samples exhibit strong magnetovolume effect around magnetic phase transition, we have calculated the barocaloric effect using the Clausius_Clapeyron relation[43]. The barocaloric effects entropy change $\Delta S_{bar}$, have been derived to be $\Delta S_{bar} = 9.6$ J/kgK, 13.5 J/kgK and 13.2 J/kgK for $TbMn_2Ge_2$,$Tb_{0.9}Y_{0.1}Mn_2Ge_2$ and $Tb_{0.8}Y_{0.2}Mn_2Ge_2$ respectively. These barocaloric values indicate that these materials can be considered as a potential candidate for mechanocaloric effects over the hydrogen and natural gas liquefaction temperature ranges.

**Heat Capacity.** The heat capacity of $TbMn_2Ge_2$ over the temperature range 2–250 K is shown in Fig. 7(a). The sharp peak in the heat capacity near the Curie temperature of $TbMn_2Ge_2$ on both zero magnetic field and a field of 2 T reflects the first order character of the magnetic phase transition. The peak in specific heat shifts from ~98 K to 102.6 K for magnetic fields of 0 T and 2 T respectively; this behaviour corresponds well to the values of the Curie temperature of $TbMn_2Ge_2$ - 97.5 K (B = 0 T ) to 103 K (B = 2 T) - obtained for the magnetization measurements (Fig. 3(d)).

The heat capacity C(T) of a metallic magnetic material includes contributions from phonons, electrons and magnons and can be described as follows:

$$C(T) = C_{ph}(T) + C_{el}(T) + C_m(T). \quad (7)$$

where $C_{ph}$, $C_{el}$ and $C_m$ are the lattice, electronic, and magnetic contributions respectively[44]. In the absence of a magnetic phase transition, the heat capacity can be described as:

$$C(T) = \gamma T + \beta T^3. \quad (8)$$

where $\gamma$ and $\beta$ are the electronic and phonon heat capacity coefficients, respectively. For the specific heat of $TbMn_2Ge_2$ at low temperatures $T \leq 1$ K, well away from the magnetic transition, as shown in Fig. 7(b), a fit to the graph of $C_p/T$ versus $T^2$ leads to $\gamma = (65.2 \pm 0.95)$mJ/molK$^2$, $\beta = (4.53 \pm 0.156) \times 10^{-4}$ J/molK$^4$. The electronic density of states $N(E_F)$ at the Fermi surface can be calculated by the formula:[44]

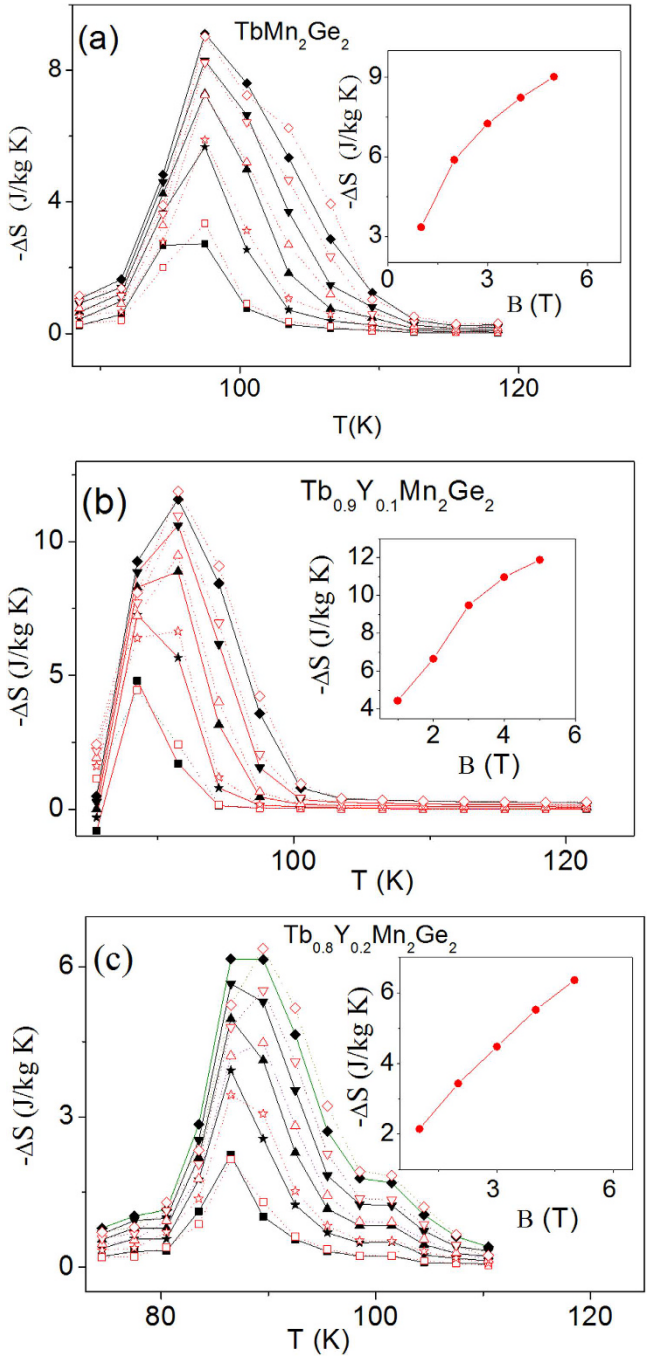


**Figure 6. The magnetic entropy changes around the ferromagnetic transition temperatures for applied magnetic fields from 1–5T.** (**a**) $TbMn_2Ge_2$, (**b**) $Tb_{0.9}Y_{0.1}Mn_2Ge_2$ and (**c**) $Tb_{0.8}Y_{0.2}Mn_2Ge_2$ (black full symbols ■ ★ ▲ ▼ ◆ for 1–5 T respectively during increasing field and the red empty symbols correspond to 1–5 T for the decreasing field). The insets show the variation of the maximum values of magnetic entropy changes for the decreasing field values.

$$\gamma = \frac{k^2_B * \pi^2}{3} N(E_F) \tag{9}$$

where $k_B$ is the Boltzmann constant. For the $TbMn_2Ge_2$ compound, the value of $N(E_F)$ is derived to be $(5.54 \pm 0.08)$ state/eV atom. Likewise, the Debye temperature $\theta_D$ can also be obtained by:

$$\beta = \frac{12 * \pi^4 * R}{5 * \theta^3_D} \cong \frac{1944 * n}{\theta^3_D} \tag{10}$$

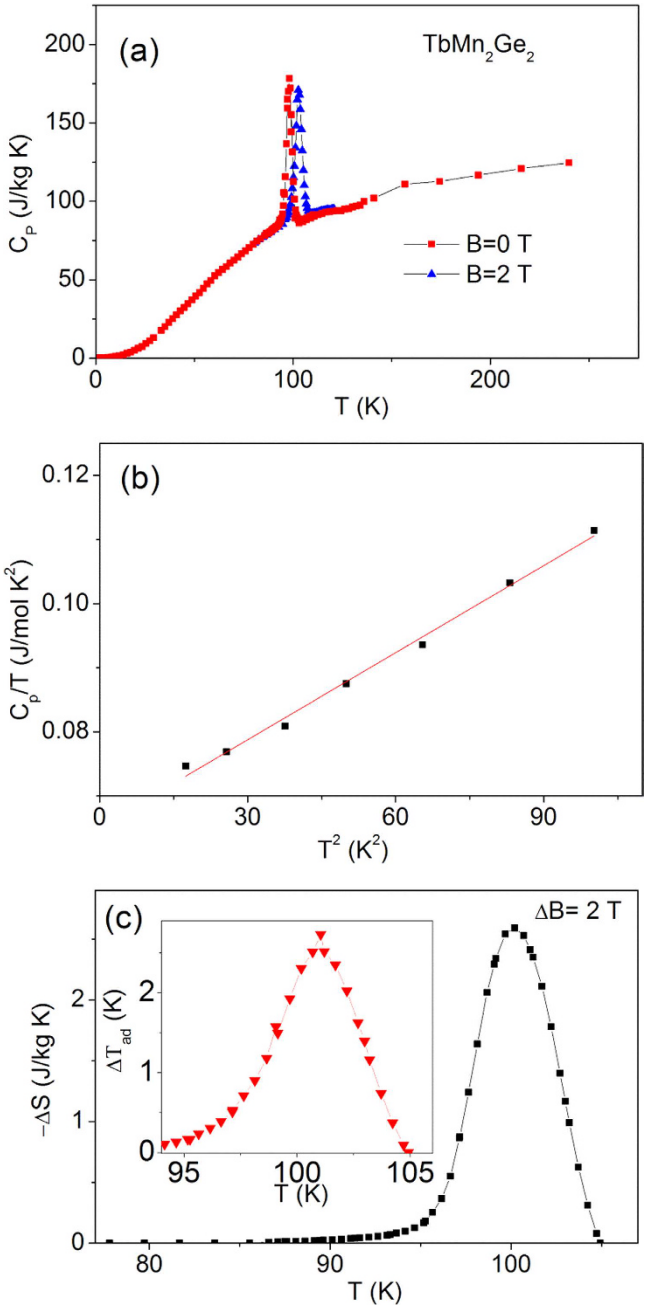


**Figure 7. The specific heat capacity relative parameters for $TbMn_2Ge_2$.** (**a**) The specific heat capacity $C_P$ of $TbMn_2Ge_2$ over the temperature range 2–250 K in zero magnetic field (red solid square) and a field of 2 T (blue solid triangle). (**b**) A graph of $C_p/T$ versus $T^2$ for $TbMn_2Ge_2$ at temperatures below 10 K. (**c**) Magnetic entropy change $-\Delta S$ as a function of temperature derived from the specific heat data of Fig. 7(a) for $\Delta B = 0$–2 T. The inset shows the corresponding adiabatic temperature change, $\Delta T_{ad}$.

where R is the universal gas constant and the number of atoms n = 5[45]. The Debye temperature for $TbMn_2Ge_2$ was determined as $\theta_D = 278 \pm 3$ K.

The magnetic entropy change, $-\Delta S_M$ (T, B) can also be derived from measurements of the in-field heat capacity using the expression thermodynamic relations below:[46]

$$\Delta S_M(T, B) = \int_0^T \frac{C(T', B) - C(T', 0)}{T'} dT' \quad (11)$$

where C(T, B) and C(T, 0) are the values of the heat capacity measured in field B and zero field, respectively. The maximum of magnetic entropy change has been derived to be $-\Delta S_M = 2.6$ J/kgK for $TbMn_2Ge_2$ (field change of $\Delta B = 2$ T), which is smaller than the value ($-\Delta S_M = 5.9$ J/kgK) deduced from the isothermal magnetization

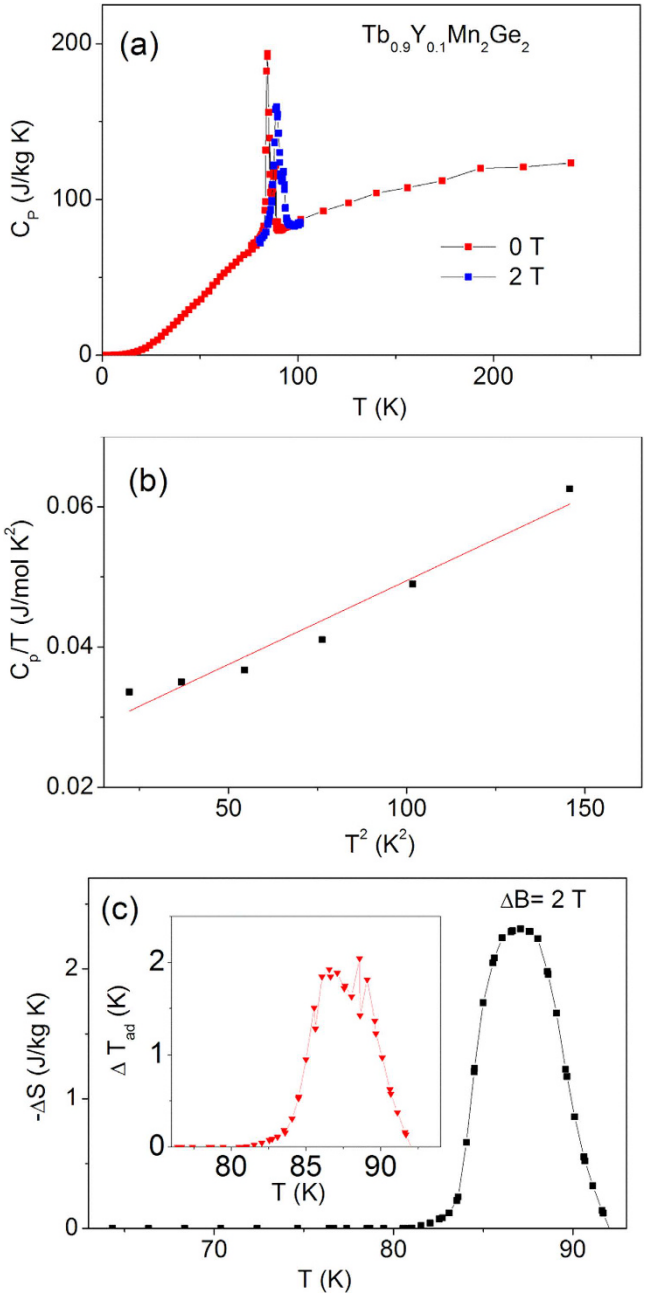


**Figure 8. The specific heat capacity relative parameters for $Tb_{0.9}Y_{0.1}Mn_2Ge_2$.** (**a**) The specific heat capacity $C_P$ of $Tb_{0.9}Y_{0.1}Mn_2Ge_2$ over the temperature range 2–250 K in zero magnetic field (red solid square) and a field of 2 T (blue solid triangle). (**b**) A graph of $C_p/T$ versus $T^2$ for $Tb_{0.9}Y_{0.1}Mn_2Ge_2$ at temperatures below 10 K. (**c**) Magnetic entropy change $-\Delta S$ as a function of temperature derived from the specific heat data of Fig. 8a for $\Delta B = 0$–2 T. The inset shows the corresponding adiabatic temperature change, $\Delta T_{ad}$.

curves. This behaviour may be due to the fact that a straightforward numerical integration using Maxwell equation based on magnetization curves is not applicable in the phase-separated state as described in ref. 47,48. The corresponding adiabatic temperature change, $-\Delta T_{ad}$ (shown as inset of Fig. 7(c) can be evaluated from $-\Delta S_M$ (T, B) and the heat capacity data.

The equivalent heat capacity parameters for $Tb_{0.9}Y_{0.1}Mn_2Ge_2$ and $Tb_{0.8}Y_{0.2}Mn_2Ge_2$ are shown in Figs 8 and 9, respectively. The Debye temperatures were found to increase from 281 K for $TbMn_2Ge_2$ to 344 K for $Tb_{0.9}Y_{0.1}Mn_2Ge_2$ and 354 K for $Tb_{0.8}Y_{0.2}Mn_2Ge_2$; with the increases understood in terms of the differences in their molecular mass[31]. The adiabatic temperature changes near the Curie temperature are found to decrease from $-\Delta T_{ad} = 2.6$ K for $TbMn_2Ge_2$, to $-\Delta T_{ad} = 2.3$ K for $Tb_{0.9}Y_{0.1}Mn_2Ge_2$ and 1.8 K for $Tb_{0.8}Y_{0.2}Mn_2Ge_2$.

The electron density at the Fermi surface is found to decrease from 5.54 state/eV atom for $TbMn_2Ge_2$ to 2.18 state/eV atom and 3.06 state/eV atom for $Tb_{0.9}Y_{0.1}Mn_2Ge_2$ and $Tb_{0.8}Y_{0.2}Mn_2Ge_2$ respectively. All the fitting results including electronic heat capacity coefficient $\gamma$, phonon heat capacity coefficient $\beta$, electronic density of

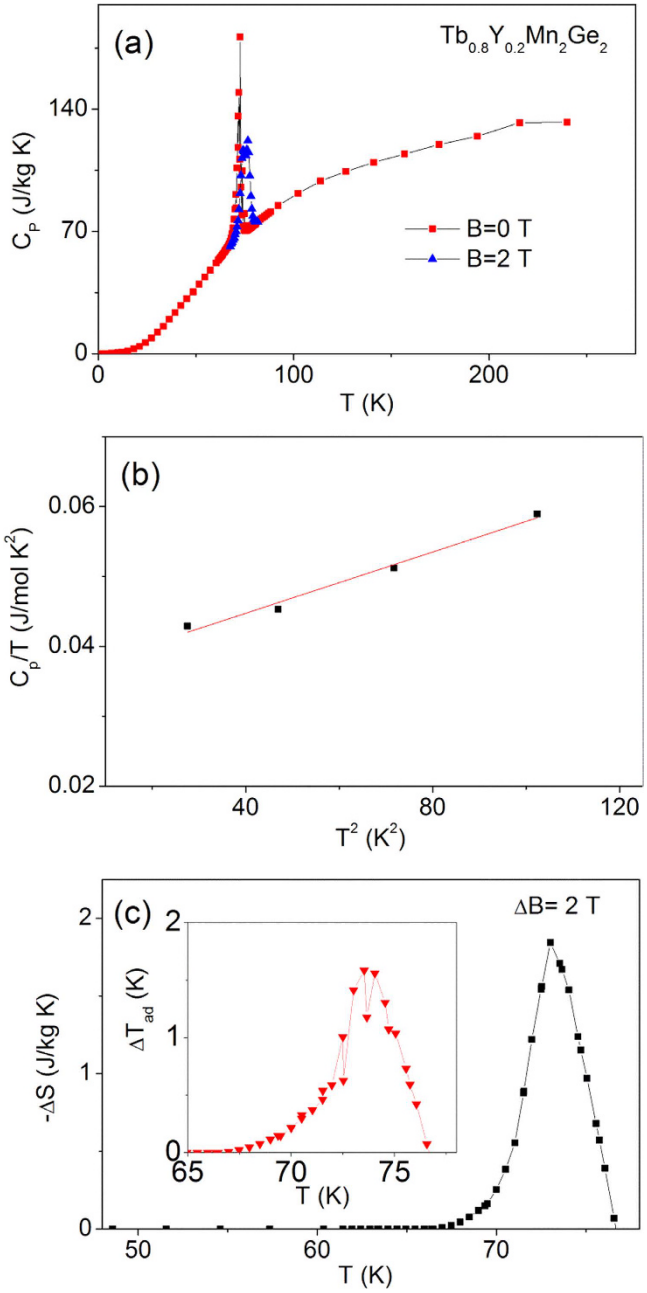


**Figure 9. The specific heat capacity relative parameters for $Tb_{0.8}Y_{0.2}Mn_2Ge_2$.** (**a**) The specific heat capacity $C_P$ of $Tb_{0.8}Y_{0.2}Mn_2Ge_2$ over the temperature range 2–250 K in zero magnetic field (red solid square) and a field of 2 T (blue solid triangle). (**b**) A graph of $C_p/T$ versus $T^2$ for $Tb_{0.8}Y_{0.2}Mn_2Ge_2$ at temperatures below 10 K. (**c**) Magnetic entropy change $-\Delta S$ as a function of temperature derived from the specific heat data of Fig. 9(a) for $\Delta B = 0$–2 T. The inset shows the corresponding adiabatic temperature change, $\Delta T_{ad}$.

states N(EF) and Debye temperature $\theta_D$ are summarized in Table 2. The modification of the electron density at the Fermi surface may be related to the difference of electronic configuration of Y and Tb as well as the unit cell size variation. The latter may lead to the variation in the degree of hybridization of Mn 3d states with p states of Ge with decreasing interatomic distances for Y doped samples. Similar behaviour has been found in the $La_{1-x}Y_xMn_2Si_2$ system where the electron density is derived to be 2.83 states/eV atom for $x = 0$, 2.51 states/eV atom for $x = 0.25$, 2.54 states/eV atom for $x = 0.3$ and 1.47 states/eV atom for $x = 1.0$[49]. Moreover, it is also noted that the electron density at the Fermi level for $TbMn_2Si_2$[29] was reported to be 2.38 states/eV atom, which is close to the values reported here for $Tb_{1-x}Y_xMn_2Ge_2$ samples.

## Conclusions

In conclusion, we have carried out a detailed investigation around the region of the magnetic transitions of compounds in the $Tb_{1-x}Y_xMn_2Ge_2$ series ($x = 0$, 0.1, 0.2) by variable temperature x-ray diffraction, heat capacity,

| x | $\gamma$ (mJ/molK$^2$) | $\beta$ (J/molK$^4$) | N($E_F$) (state/eV atom) | $\theta_D$ (K) |
|---|---|---|---|---|
| 0 | $65.2 \pm 0.9$ | $(4.53 \pm 0.16) \times 10^{-4}$ | $5.54 \pm 0.08$ | $278 \pm 3$ |
| 0.1 | $25.6 \pm 2.0$ | $(2.39 \pm 0.24) \times 10^{-4}$ | $2.18 \pm 0.17$ | $345 \pm 12$ |
| 0.2 | $36.0 \pm 1.3$ | $(2.19 \pm 0.19) \times 10^{-4}$ | $3.06 \pm 0.11$ | $355 \pm 11$ |

**Table 2. Calculated heat capacity parameters for $Tb_{1-x}Y_xMn_2Ge_2$ (x = 0, 0.1, 0.2).** Electronic heat capacity coefficient $\gamma$, phonon heat capacity coefficient $\beta$, electronic density of states N($E_F$) and Debye temperature $\theta_D$.

differential scanning calorimetry and magnetic measurements. Two magnetic phase transitions occur at $T_N^{inter}$ and $T_C^{inter}$ for each of the three samples. The antiferromagnetic transition at $T_N^{inter}$ is shown to increase slightly with increase in the Y concentration, while the ferromagnetic transition at $T_C^{inter}$ drops significantly. The mechanism of reduction of $T_C$ due to the substitution of Y for Tb has been analysed and chemical pressure is found to play a significant role. Moreover, the entropy change of $Tb_{0.9}Y_{0.1}Mn_2Ge_2$ is found to exhibit very good magnetocaloric performance around $T_C^{inter}$ ($-\Delta S = 11.9\,J\,kg^{-1}\,K^{-1}$ and RCP = 102.9 J kg$^{-1}$ for a field change of $\Delta B = 0$–5 T) with a small hysteresis loss of 5.36 J/kg. This behaviour reflects the potential suitability of $Tb_{0.9}Y_{0.1}Mn_2Ge_2$ for operation as a magnetic refrigerant below the nature gas liquefaction temperature. The Debye temperature and the density of states N($E_F$) at the Fermi level have been determined and analyzed from the heat capacity.

## References


1. Pecharsky, V. K. & Gschneidner, K. A. Giant Magnetocaloric Effect in $Gd_5(Si_2Ge_2)$. *Physical Review Letters* **78,** 4494 (1997).
2. Gschneidner Jr, K. A., Pecharsky, V. K. & Tsokol, A. O. Recent developments in magnetocaloric materials. *Reports on Progress in Physics* **68,** 1479–1539 (2005); Gschneidner Jr, K. A. and Pecharsky, V. K. Thirty years of near room temperature magnetic cooling: Where we are today and future prospects. *International Journal of Refrigeration* **31**, 945–961 (2008); Shen, B. G. *et al.*, Recent Progress in Exploring Magnetocaloric Materials. *Advanced Materials* **21,** 4545–4564 (2009).
3. Tegus, O., Brück, E., Buschow, K. H. J. & de Boer, F. R. Transition-metal-based magnetic refrigerants for room-temperature applications. *Nature* **415,** 150–152 (2002).
4. Wada, H. & Tanabe, Y. Giant magnetocaloric effect of $MnAs_{1-x}Sb_x$. *Applied Physics Letters* **79,** 3302 (2001).
5. Krenke, T. *et al.* A. Inverse magnetocaloric effect in ferromagnetic Ni–Mn–Sn alloys. *Nature materials* **4,** 450– 454 (2005).
6. Hu, F. X., Shen, B. G. Sun, J. R. & Wu, G. H. Large magnetic entropy change in a Heusler alloy $Ni_{52.6}Mn_{23.1}Ga_{24.3}$ single crystal, *Physical Review B* **64,** 132412 (2001).
7. Pasquale, M. *et al.* Magnetostructural transition and magnetocaloric effect in $Ni_{55}Mn_{20}Ga_{25}$ single crystals. *Physical Review B* **72,** 094435 (2005).
8. Zhang, X. X. *et al.* Magnetic entropy change in Fe-based compound $LaFe_{10.6}Si_{2.4}$. *Applied Physics Letters* **77,** 3072 (2000); Hu, F.X. *et al.*, Influence of negative lattice expansion and metamagnetic transition on magnetic entropy change in the compound $LaFe_{11.4}Si_{1.6}$. *Applied Physics Letters* **78,** 3675 (2001).
9. Casanova, F. *et al.* Effect of a magnetic field on the magnetostructural phase transition in $Gd_5(Si_xGe_{1-x})_4$. *Physical Review B* **69,** 104416 (2004).
10. von Ranke *et al.* Magnetocaloric effect in the $RNi_5$ (R = Pr, Nd, Gd, Tb, Dy, Ho, Er) series. *Physical Review B* **70,** 134428 (2004).
11. Zeng, R., Dou, S. X., Wang, J. L. & Campbell, S. J. Large magnetocaloric effect in re-entrant ferromagnet $PrMn_{1.4}Fe_{0.6}Ge_2$. *Journal of Alloys and Compounds* **509,** L119–L123 (2011).
12. Wang, L. C. *et al.* Low-temperature large magnetocaloric effect in the antiferromagnetic CeSi compound. *Journal of Alloys and Compounds* **587,** 10–13 (2014).
13. Maji, B., Ray, M. K., Suresh, K. G. & Banerjee, S. Large exchange bias and magnetocaloric effect in $TbMn_2Si_2$. *Journal of Applied Physics* **116,** 213913 (2014).
14. Samanta, T., Das, I. & Banerjee, S. Giant magnetocaloric effect in antiferromagnetic $ErRu_2Si_2$ compound. *Applied Physics Letters* **91,** 152506 (2007).
15. Wang, J. L. *et al.* Driving Magnetostructural Transitions in Layered Intermetallic Compounds. *Physical Review Letters* **110,** 217211 (2013).
16. Zuo, W. L., Hu, F. X., Rong, S. J. & Shen, B. G. Low-field large reversible magnetocaloric effect in the $RNi_2Si_2$ (R = Dy, Ho, Er) compounds. *Journal of Magnetism and Magnetic Materials* **344,** 96–100 (2013).
17. Li, L. *et al.* Low-field giant reversible magnetocaloric effect in intermetallic compound $ErCr_2Si_2$. *Scripta Materialia* **67,** 237–240 (2012).
18. Ban, Z. & Sikirica, M. The crystal structure of ternary silicides $ThM_2Si_2$ (M = Cr, Mn, Fe, Co, Ni and Cu) Acta Crystallographica **18,** 594–599 (1965).
19. Purwanto, S. *et al.* The effects of dilution on the competing exchange state in (Tb, Y)$Mn_2X_2$ (X = Ge, Si). *Physica B.* **213,214,** 318–320 (1995).
20. Granovsky, S. A. *et al.* The magnetic structures and the magnetic phase diagram of the $TbMn_2(Ge, Si)_2$ system. *Physica B* **391,** 79–87 (2007).
21. Brabers, J. H. V. J. *et al.* Strong Mn-Mn distance dependence of the Mn interlayer coupling in $SmMn_2Ge_2$-related compounds and its role in magnetic phase transitions. *Physical Review B* **50,** 16410 (1994).
22. Venturini,G., Welter, R., Ressouche, E. & Malaman, B. Neutron diffraction study of $Nd_{0.35}La_{0.65}Mn_2Si_2$: A $SmMn_2Ge_2$-like magnetic behaviour compound. *Journal of Magnetism and Magnetic Materials* **150,** 197 (1995).
23. Morellon, L., Algarabel, P. A., Ibarra, M. R. & Ritter, C. Magnetic structures and magnetic phase diagram of $Nd_xTb_{1-x}Mn_2Ge_2$. *Physical Review B* **55,** 12363 (1997).
24. Purwanto, S., Oihashi, M., Yamauchi, H., Onodem, H. & Yamaguchr, Y. *Prosiding PertemuanI lmiah Sains Materi* 1410 (1997).
25. Ott, H. R. & Fisk, Z. *Handbook on the Physics and Chemistry of the Actinides*, (ed. Freeman, A. J. & Lander, G. H.) 85 (1987).
26. Szytula, A. & Leciejewicz, J. *Handbook on the Physics and Chemistry of Rare Earths* (ed. Gscheidner Jr, K. A. & Eyring, L.) 133 (1989).
27. Kolmakova, N. P., Sidorenko, A. A. & Levitin, R. Z. Features of the magnetic properties of rare-earth intermetallides $RMn_2Ge_2$. *Low Temperature Physics* **28,** 653 (2002).
28. Kumar, P. *et al.* Pressure-induced changes in the magnetic and magnetocaloric properties of $RMn_2Ge_2$(R = Sm, Gd). *Physical Review B* **77,** 224427 (2008).
29. Li, G. X. *et al.* Large entropy change accompanying two successive magnetic phase transitions in $TbMn_2Si_2$ for magnetic refrigeration. *Applied Physics Letters* **106,** 182405 (2015); Li, L. W. *et al.* Giant reversible magnetocaloric effect in $ErMn_2Si_2$ compound with a second order magnetic phase transition. Applied Physics Letters **100,** 152403 (2012).

30. Dubenko, I. S., Gaidukova, I. Y., Granovsky, S. A., Inoue, K. & Markosyan, A. S. Magnetic phase transitions in (Tb,Y) $Mn_2M2$ (M = Ge and Si) Systems. *Journal of Applied Physics* **93,** 10 (2003).
31. McCusker,. L. B. *et al.* Rietveld refinement guidelines. *Journal of Applied Crystallography* **32,** 36–50 (1999).
32. Wang, J. L. *et al.* Magnetocaloric effect in layered $NdMn_2Ge_{0.4}Si_{1.6}$. *Applied Physics Letters* **98,** 232509 (2011).
33. Md, Din *et al.* Magnetic properties and magnetocaloric effect of $NdMn_{2-x}Ti_xSi_2$ compounds. *Journal of Physics D: Applied Physics* **46(44),** 1–11 (2013).
34. Md, Din *et al.* Magnetic phase transitions and entropy change in layered $NdMn_{1.7}Cr_{0.3}Si_2$. *Applied Physics Letters* **104,** 042401 (2014).
35. Matsunami, D., Fujita, A., Takenaka, K. & Kano, M. Giant barocaloric effect enhanced by the frustration of the antiferromagnetic phase in $Mn_3GaN$. *Nature Material* **14,** 73–78 (2015).
36. Wang, J. L. *et al.* Phase gap in pseudoternary R1−yRyMn2X2−xXx compounds. *Physical Review B* **87,** 104401 (2013).
37. Kennedy, S. J., Wang, J. L., Campbell, S. J., Hofmann, M. & Dou, S. X. Pressure induced magneto-structural phase transitions in layered $RMn_2X_2$ compounds. *Journal of Physics* **115,** 172617 (2014).
38. Morellon, L., Arnold, Z., Kamarad, J., Ibarra, M. R. & Algarabel, P. A. The magnetic phase transitions and related volume changes in $(Nd_{1-x}Tb_x)Mn_2Ge_2$ compounds. *Journal of Magnetism and Magnetic Materials* **177,** 1085–1086 (1998).
39. Ray, M. K., Bagani, K. & Banerjee, S. Effect of excess Ni on martensitic transition, exchange bias and inverse magnetocaloric effect in $Ni_{2+x}Mn_{1.4-x}Sn_{0.6}$ alloy. *Journal of Alloys and Compounds* **600,** 55–59 (2014).
40. Parra-Borderias, M., Bartolome, F., Herrero-Albillos, J. & Garcia, L. M. Detailed discrimination of the order of magnetic transitions and magnetocaloric effect in pure and pseudobinary Co Laves phases. *Journal of Alloys and Compounds* **481,** 48 (2009).
41. Bonilla, C. M. *et al.* A new criterion to distinguish the order of magnetic transitions by means of magnetic measurements. *Journal of Applied Physics* **107,** 09E–131 (2010).
42. Mañosa, L. *et al.* Giant solid-state barocaloric effect in the Ni-Mn-In magnetic shape memory alloy. *Nature Mater* **9,** 478–481 (2010).
43. Matsunami, D., Fujita, A., Takenaka, K. & Kano, M. Giant barocaloric effect enhanced by the frustration of the antiferromagnetic phase in $Mn_3GaN$. *Nature Material* **14,** 73–78 (2015).
44. Bouvier, M., Lethuillier, P. & Schmitt, D. Specific heat in some gadolinium compounds. I. Experimental. *Physical Review B* **43,** 13137 (1991).
45. Emre, B., Dincer, I. & Elerman, Y. Analysis of heat capacity and magnetothermal properties of the $La_{0.775}Gd_{0.225}Mn_2Si_2$ compound. *Intermetallics* **31,** 16–20 (2012).
46. Nirmala, R., Morozkin, A. V. & Malik, S. K. Magnetism and heat capacity of $Dy_5Si_2Ge_2$. *Physical Review B* **75,** 094419 (2007).
47. Liu, G. J. *et al.* Determination of the entropy changes in the compounds with a first-order magnetic Transition. *Applied Physics Letters* **90,** 032507 (2007).
48. Caron, L. *et al.* On the determination of the magnetic entropy change in materials with first-order transitions. *Journal of Magnetism and Magnetic Materials* **321,** 3559–3566 (2009).
49. Gerasimov, E. G., Gaviko, V. S. & Kanomat, T. Heat capacity of $La_{1-x}Y_xMn_2Si_2La_{1-x}Y_xMn_2Si_2$ compounds. *Journal of Magnetism and Magnetic Materials* **310,** e563–e565 (2007).


## Acknowledgements

Z. X. Cheng thanks the Australia Research Council for Future Fellowship (FT0990391). This work was supported in part by Australia Research Council Discovery Grant No. DP110102386. The authors thank Dr. T. Silver for his contribution to English expression.

## Author Contributions

J.L. Wang and Z.X. Cheng designed the project. C.S. Fang, G. X Li, J.L. Wang, W.D. Hutchison, Z.X. Cheng and Q.Y. Ren carried out the experimental work. C.S. Fang, J.L. Wang, Z.X. Cheng and S.J. Campbell wrote the paper. All the authors interpreted and discussed the work.

## Additional Information

**Competing Interests:** The authors declare no competing financial interests.

**How to cite this article:** Fang, C. *et al.* New insight into magneto-structural phase transitions in layered $TbMn_2Ge_2$-based compounds. *Sci. Rep.* **7**, 45814; doi: 10.1038/srep45814 (2017).

**Publisher's note:** Springer Nature remains neutral with regard to jurisdictional claims in published maps and institutional affiliations.